Electrospun HPMC/PEO-blend orodispersible films: how slight batch differences affect the crucial mechanical properties

**Nikifor Asatiani · Barbora Filipová ·
Miroslava Pechočiaková · Anna Kluk ·
Štepán Kunc · Petr Mikeš**

Abstract Orodispersible films comprise a promising dosage form with a wide range of advantages compared to conventional formulations. The electrospinning process can significantly enhance the relevant characteristics of orodispersible films, e.g., the dissolution rate and the ease of administration. This study involved the use of two types of hydroxypropyl methylcelluloses of low molecular weight obtained from three different manufacturers as the matrix. The SEM, FTIR, RAMAN, and DSC analyses revealed comparable values for all the fabricated materials. However, the mechanical properties of the fibers differed significantly, with electrospun Methocel E5/ PEO proving to be particularly brittle. This is probably caused by the different arrangements of substituted methoxy- and hydroxypropyl groups of studied HPMCs. It is hoped that this paper will serve as an example of the extent to which slight differences between HPMC powder batches can dramatically alter the key properties of electrospun orodispersible films.

Keywords Orodispersible films · Hypromellose · Nanofibers · Mechanical properties

N. Asatiani · B. Filipová · Š. Kunc · P. Mikeš (✉)
Department of Physics, The Faculty of Science,
Humanities and Education, Technical University
of Liberec, Studentská 1402/2, 461 17 Liberec,
Czech Republic
e-mail: petr.mikes@tul.cz

N. Asatiani
e-mail: nikifor.asatiani@tul.cz

B. Filipová
e-mail: Barbora.filipova@tul.cz

Š. Kunc
e-mail: stepan.kunc@tul.cz

M. Pechočiaková
Department of Material Engineering, Faculty of Textile
Engineering, Technical University of Liberec, Studentská
1402/2, 461 17 Liberec, Czech Republic
e-mail: miroslava.pechociakova@tul.cz

A. Kluk
Zentiva, K.S., U Kabelovny 130, Prague 10,
Prague 102 00, Czech Republic
e-mail: anna.kluk@zentiva.com

Introduction

Orodispersible films (ODFs) comprise a relatively new and particularly promising dosage form. This dosage form is suitable for patients with swallowing difficulties (dysphagia), especially for the elderly and young children (Preis 2015; Slavkova and Breitkreutz 2015; Orlu et al. 2017; Visser et al. 2017). Therefore, pharmaceutical companies are engaged in the development of various innovative oral dosage forms, one of the most promising of which comprises FDS (Fast dissolving system), which allows for very rapid dispersion in the oral cavity. The major advantages of these systems concern their simple discrete administration without the need for swallowing or chewing

and the rapid onset of action (Bala et al. 2013; Bahrainian et al. 2017). The various systems include tablets, films, wafers, and buccal and sublingual patches, which can be used for topical and systemic drug delivery purposes (Bahrainian et al. 2017). According to European Pharmacopoeia, ODFs are defined as "*single or multilayer sheets of suitable materials, to be placed in the mouth where they disperse rapidly* ", i.e. within 30 s (Council of Europe. 2019). The most commonly used oral film-delivery drugs consist of anesthetics, cough, and sore throat medications, antiasthmatics, and antihistamines, as well as erectile dysfunction, gastrointestinal, nausea, and CNS medication drugs. Other injectables include caffeine, various vitamins, and sleeping and snoring medications (Borges et al. 2015; Irfan et al. 2016; Mahboob et al. 2016). This dosage form is particularly suitable for highly-potent drugs administered in low doses (Hoffmann et al. 2011).

The main advantages of ODFs consist of rapid dissolution and disintegration (with nanofibrous films this advantage is multiplied) and the subsequent onset of the action of the drug, simple and discreet administration without the need for water, high dosing efficacy and accuracy, etc. (Bala et al. 2013; Irfan et al. 2016; Mahboob et al. 2016; Bahrainian et al. 2017). The disadvantage of these films remains however the limitation of the dose of the drug, which is up to 100 mg (Borges et al. 2015); furthermore, due to their good water solubility, ODFs need to be protected from moisture, ideally with aluminum foil or another barrier material.Oral dispersion films are most commonly produced via methods involving casting (pouring) and drying, e.g., solvent casting and semi-solid casting. Other fabrication methods include extrusion, including hot-melt extrusion and solid dispersion extrusion, and the 3D printing method (Borges et al. 2015; Irfan et al. 2016; Effiong Daniel Ekpa et al. 2020). Moreover, in recent years, the trend toward the fabrication of nanofibers via electrospinning has gained considerable momentum in this field. The solvent casting method is based on the spreading of a polymer matrix over a support substrate and the subsequent drying/removal of the solvent in an oven. The active pharmaceutical ingredient (API) is dissolved or suspended in a solution of polymers, plasticizers, disintegrants, and other components that are soluble in a volatile solvent, most commonly water or alcohol. The disadvantage of this method however concerns

the potential presence of residual solvents in the film if a solvent other than water is used (Borges et al. 2015).

Electrospinning, including the needleless DC electrospinning approach, provides for the preparation of ODFs in the form of nanofibers. This method involves the application of an external electric field to a polymer solution that is deposited on a thin string. The polymer solution is then broken down via Rayleigh-Plateau instability into individual droplets from which an electric field, following the overcoming of capillary forces, generates a jet that is subsequently elongated to nanometer dimensions and deposited on the so-called collector (Lin and Wang 2013). The main advantage of nanofibrous layers compared to conventional methods concerns their large specific surface, which significantly reduces the dissolution time of the layer. However, this may also be a disadvantage in terms of industrial production due to the high susceptibility of such layers to atmospheric humidity and problems with storage. A further advantage is that the process involves the massive evaporation of solvents and, thus, almost no residual solvents remain within the fibers. As with the more commonly used ODF preparation methods, industrial production allows for considerable cost savings.

The choice of polymeric agents (usually a combination of at least 2 polymers) for the formation of oral films is particularly important. It is necessary to ensure the good mechanical properties of the resulting film, rapid dissolution, and compatibility of the polymers themselves.

The stability of the material depends on the polymer and the overall composition of the film. The potential occurrence of phase separation and the crystallization of the polymer or API (active pharmaceutical ingredient) results in the deterioration of the mechanical properties of oral films, which negatively influences post-production processing including slicing, packaging, and handling during the delivery of the drug. A study by Samprasit et al. (2015), which investigated the physical stability of nanofibrous PVP oral films containing Meloxicam, demonstrated that the storage of manufactured films under the appropriate conditions (25 °C/60% RH) prevents the formation of morphological crystals and ensures that the film remains stable for 6 months. The tensile strength of oral films ranges from 0.9 ± 0.4 to 1.7 ± 0.7 MPa. Interestingly, a

study by Bukhary et al. (2018) of PVP nanofibers containing Valsartan and amlodipine besylate determined a period of stability of up to 4 months before the occurrence of phase separation. Paaver et al. (2015) addressed the production of controlled-release ODF nanofibers. Their comparison of 3 HPMCs containing Piroxicam determined that the recrystallization of APIs occurs over time and that the process is accelerated at low temperatures and humidity levels. Thus, the quality of nanofibrous films depends on the quality of the HPMC, the solvent system, and the storage conditions. Similar results were obtained by Bin et al. (2014) in their investigation of the effect of HPMC, PVP, and the plasticizer concentration on the production of nanofibrous ODFs with Donepezil HCl. The tensile strength was found to increase with higher HPMC concentrations, the plasticizers acted to decrease the strength but increased the elasticity (with optimum amounts and types), and the PVP content in the composition of the film served to enhance both the strength and elasticity of the material. Tort and Acartürk (2016) prepared a nanofibrous ODF with HPMC, PEO, and sodium alginate with the addition of glutamine. The highest degree of elongation was achieved by Birer and Acartürk (2021) for nanofibrous films containing telmisartan and L-Arginine using a PVP matrix. The results revealed that the films produced via electrospinning had a higher Young's modulus E and exhibited a deterioration in their mechanical properties after 1 month. The nanofibrous films were also found to exhibit a deterioration in the dissolution rate over time due to the recrystallization of the drug within the fibers.

This article provides a summary of the testing of several HPMCs, for which a high-productivity polymer system was specially designed based on non-toxic solvents. We show that the sourcing of polymers with the same parameters from different manufacturers can significantly influence the mechanical properties of the fabricated layers. We hypothesize that even slight differences between arrangements of substituted methoxy- and hydroxy-propyl groups of HPMC can dramatically alter the critical properties of electrospun ODFs. In the previous study by Švára et al. (2022) APIs, specifically tadalafil, were added to the nanofibrous layer and several properties were studied with an emphasis on mechanical properties. In this paper, only the matrix

has been studied to exclude intermolecular interaction between the polymers and the API.

Materials and methods

Materials

Polyethylene oxide with a molecular weight of 100 kDa was purchased from Sigma Aldrich. Hypromellose Methocel E5 was purchased from JRS Pharma (Rosenberg, Germany); the viscosity value of aqueous 2% (w/v) solution at 20 °C was 5 mPas. Pharmacoat 606 was purchased from Shin-Etsu Chemical (Tokyo, Japan); the viscosity value of aqueous 2% (w/v) solution at 20 °C was 6 mPas. Tylopur 605 and 606 were purchased from SE Tylose (Wiesbaden, Germany); the viscosity value of aqueous 2% (w/v) solution at 20 °C was 5 and 6 mPa s, respectively. Methoxyl content was 28–30% and a hydroxypropoxyl content of 7–12% for all the tested HPMCs. The purified water and Isopropyl alcohol were obtained from Penta chemicals (Czech Republic).

Fabrication of the nanofibrous ODFs

The spinning solutions were prepared via the dispersion of 7% (w/w) of HPMC and 3% (w/w) of PEO in isopropyl alcohol (IPA). The total volume of the solvent system was then adjusted using purified water to obtain a final IPA/water ratio of 1:1 (w/w). The polymer solutions were subsequently stirred using a magnetic stirrer (Heidolph, Schwebach, Germany) at 300 RPM for 24 h to attain complete dissolution. The solutions were then electrospun using a Nanospider® NS 1WS500U (Elmarco, Liberec, Czech Republic) needleless electrospinning machine. The parameters of the electrospinning process were set as follows: positive voltage on the spinning electrode, 40 kV; negative voltage on the collector, − 10 kV; distance between the spinning electrode and collector, 140 mm. The temperature and relative humidity were maintained at 22 ± 3 °C and 18–22%, respectively. A nonwoven (spunbond) polypropylene material was used as the substrate.

Preparation of ODFs via the film-casting method

The procedure used for the preparation of the HPMC/PEO electrospinning solution was repeated for the preparation of the film-casting solutions. However, since the 10% (w/w) polymer solutions were not sufficiently viscous to cast a smooth film, a higher concentration of 15% (w/w) was required. Around 2 ml of the stock 15%-solution was then poured onto a glass plate (10 cm × 10 cm) and a stainless-steel micrometer adjustable film applicator (TQC Sheen, Leominster, UK) with a width of 100 mm was used to obtain a smooth flat polymeric film. The casting gap was adjusted to 500 μm. The films were stored in a fume hood for 24 h at room temperature to allow for the solvents to completely evaporate.

Characterization of the morphology

Polarized light microscopy was performed using an Olympus BX-60 (Olympus, Center Valley, Pennsylvania) microscope equipped with polarized filters and 10×, 20×, and 50× objectives. Macroscopic images of the ODF surfaces were captured using a Levenhuk DTX 90 (Levenhuk, Tampa, USA) USB microscope. The morphology of the electrospun layers was analyzed using a TESCAN Vega 3SB (Brno, Czech Republic) scanning electron microscope. The fiber diameters were subsequently determined employing an ImageJ (National Institutes of Health, MD, USA) image analyzer via the measurement of 100 randomly observed nanofibers selected over different fields of view at a magnification of 5000×. The thicknesses of the nanofibrous layers were determined using a digital micrometer. The areal density (productivity), g/mm^2, of the nanofibrous layers was determined from the average weight of 5 samples with areas of 4.84 cm^2 (2.2 × 2.2 cm).

Mechanical properties of the electrospun nanofibrous layers

Tensile properties of the tested electrospun HPMC/PEO layers (particularly Young's modulus, tensile stress at maximum load, and elongation at break) are summed up in Table 1 and compared in Fig. 6 (panels B–D). The mechanical properties of the electrospun nanofibrous layers were tested for tensile strength, Young's modulus, and elongation at break. The measurements were conducted using a LaborTech LabTest 2.010 (Opava, Czech Republic) tensile tester applying the following parameters: gauge length, 50 mm, and strain rate, 100 mm/min. The fibrous layers were cut with scissors into 10 × 50 mm rectangles (plus 10 mm on either end for the clamping of the samples). The thickness of the layers was determined using a digital micrometer ($n = 10$). The tensile stress was defined as the ratio between the applied force and the sectional area of the sample (width of the sample multiplied by the thickness). The strain was defined as the ratio between the gauge displacement and the initial gauge distance. Eight samples were tested for each material to determine the average values and standard deviations.

Differential scanning calorimetry

A differential scanning calorimeter (Mettler Toledo Star 3, USA) was used for the investigation of the crystallization and melting behavior of the studied materials. The heating/cooling rate was set at 15 °C/min within a temperature range of 25–200 °C. This temperature ramping was chosen to minimize the time delay between layer production and subsequent measurement. Each sample (around 10 mg) was first heated from 25 to 200 °C and subsequently cooled to 25 °C; an empty sample pan was used as the reference. The area of the peak (normalized per sample unit weight) was determined in DSC

Table 1 Tensile profiles of the electrospun HPMC/PEO nanofibrous layers

Sample	Young modulus (MPa)	Tensile stress at maximum load (MPa)	Elongation at break (%)
E5/PEO NF	75.85 ± 13.91	1.60 ± 0.63	2.88 ± 0.96
PH606/PEO NF	57.10 ± 2.31	1.76 ± 0.04	6.43 ± 0.94
T605/PEO NF	75.42 ± 2.67	2.12 ± 0.13	5.48 ± 0.86
T606/PEO NF	63.41 ± 2.51	1.89 ± 0.05	7.05 ± 0.68

thermograms. The crystallization temperature (T_{cc}) and the cold crystallization enthalpy (ΔH_{cc}) of the samples were determined from the cooling scan, while the melting temperature (T_m) and melting enthalpy (ΔH_m) were ascertained from the heating scan.

Raman spectroscopy

A DXR™ Raman microscope (Thermo Scientific, USA) with a 532 nm laser was used for the analysis of 2 HPMC powders. The instrument was calibrated automatically before each reading. The readings, which consisted of one scan, were taken at a power of 1.5–2.0 mW with a spectral region of 3500 cm^{-1} to 100 cm^{-1}. The Raman spectra were normalized using the standard normal variate (SNV) normalization method by subtracting each spectrum by its own mean and dividing it by its own standard deviation.

Infrared-spectroscopy—FTIR

The materials were characterized using a Fourier transform spectrometer (Nicolet iZ10; Thermo Fisher, USA). A background reading was taken before each of the measurements. The samples were placed on the ATR diamond crystal for analysis, and the spectrum

analysis was collected at 25 °C using 16 scans in the infrared region in the range 400–4000 cm^{-1} and with a spectral resolution of 4 cm^{-1}.

Statistical analysis

The normality of the fiber diameter data was verified by means of Shapiro–Wilk's test and the homoscedasticity by means of Levene's test (significance level of 0.05). The statistical significance of the differences between the nanofibrous layers was analyzed via non-parametric analysis (the Kruskal–Wallis test for multiple comparisons) with Dunn's post-hoc test whenever either the assumption of normality or homoscedasticity was violated. The fiber diameter data were also expressed as the median and the interquartile range (IQR = Q3–Q1).

Results and discussion

Characterization of the morphology

Electrospun nanofibrous layers

The electrospinning processing parameters and the ambient conditions were kept constant during the
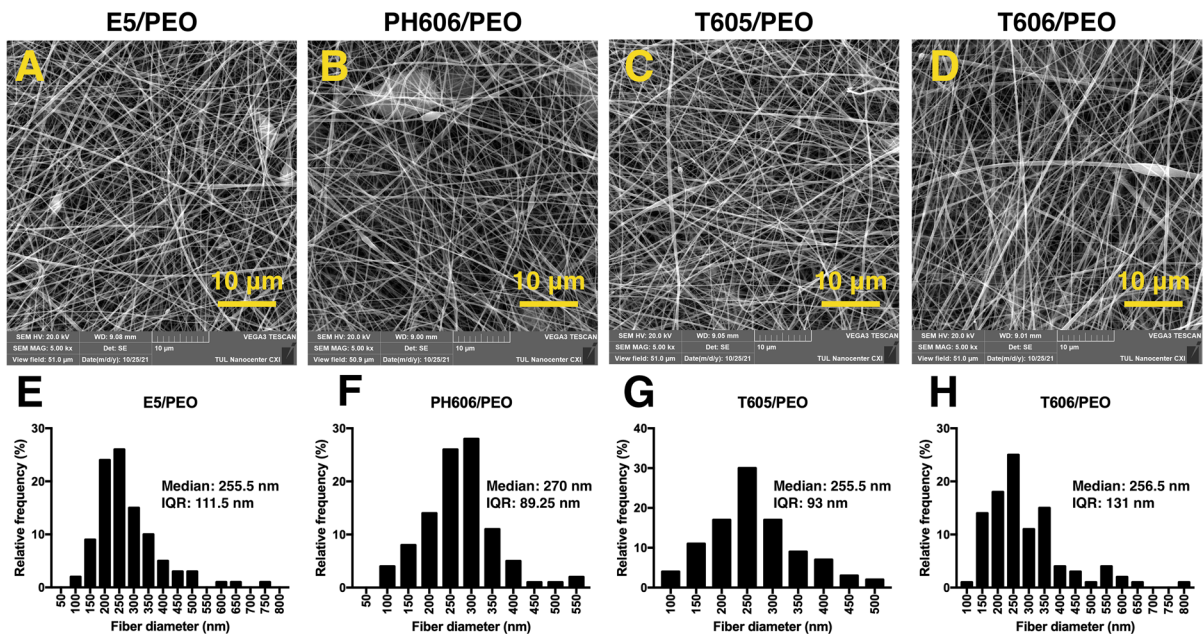

Fig. 1 Morphology of the electrospun HPMC layers. SEM images (**A–D**) and histograms of the fiber diameter distributions (**E–H**) of the electrospun fibers produced from the various HPMCs with PEO

study to ensure that the type of HPMC was the only variable parameter that affected the fiber morphology. The nanofibrous layers produced appeared to be regular and without any remarkable defects or significant differences in the macroscopic structures of the layers. Figure 1 shows representative SEM images of the obtained fibrous layers (a–d) and the distributions of the fiber diameters within the structures.

The analysis of the SEM images revealed that all the resulting electrospun fibers were free of beads and evinced fiber diameters of around 250 nm (median value, $n = 100$) with relatively limited fiber diameter distributions (generally up to 650 nm).

The observations were similar to those suggested by the data reported earlier for various electrospun HPMCs with differing PEO ratios (Aydogdu et al. 2018). On the other hand, the diameter values obtained in this study were approximately four times smaller than the HPMC/PEO fiber values obtained by Balogh et al. (2016) by means of DC electrospinning. Balogh et al. (2016), however, considered significantly lower PEO 100 k ratios (up to 5% w/w). Since none of the material fiber distributions evinced a normal distribution, the Kruskal–Wallis test was applied, which confirmed the absence of statistically significant differences ($p = 0.7492$) between the fiber diameter distributions. A marked difference was observed in terms of the productivity (mg/cm²) of the fibrous layers produced. The highest productivity, 3.27 ± 0.16 mg/cm², was determined for the T605/PEO layer, which corresponds to a high fiber density (see Fig. 1c). The productivity of the PH606/PEO and T606/PEO layers was comparable at 2.93 ± 0.20 and 2.96 ± 0.21 mg/cm², respectively, and the E5/PEO layer evinced the lowest productivity, i.e. 2.44 ± 0.24 mg/cm². The productivity was determined via the weighing of 2.2×2.2 cm samples that were stamped at three randomly selected locations for each polymer on the fabricated layer. The nanofiber layer production parameters were the same for all the nanofibrous layers.

Solvent-cast ODFs

Thin films (solid dispersions) of the same polymer formulations were solvent-cast on glass slides and analyzed by means of crossed-polarized microscopy aimed at obtaining visualizations of the phase and state transitions of the polymers used in the studied HPMC/PEO matrices. All the HPMC/PEO formulation samples revealed two distinct phases following complete drying. Three HPMCs, i.e. PH606/PEO, T605/PEO, and T606/PEO (Fig. 2b/f, c/g, d/h) evinced similar macroscopic structure patterns with highly-defined dispersion phases and dispersed bubble-like structures within. However, the E5/PEO sample (Fig. 2a/e) was more homogeneous and lacked a well-defined separated phase size and shape.

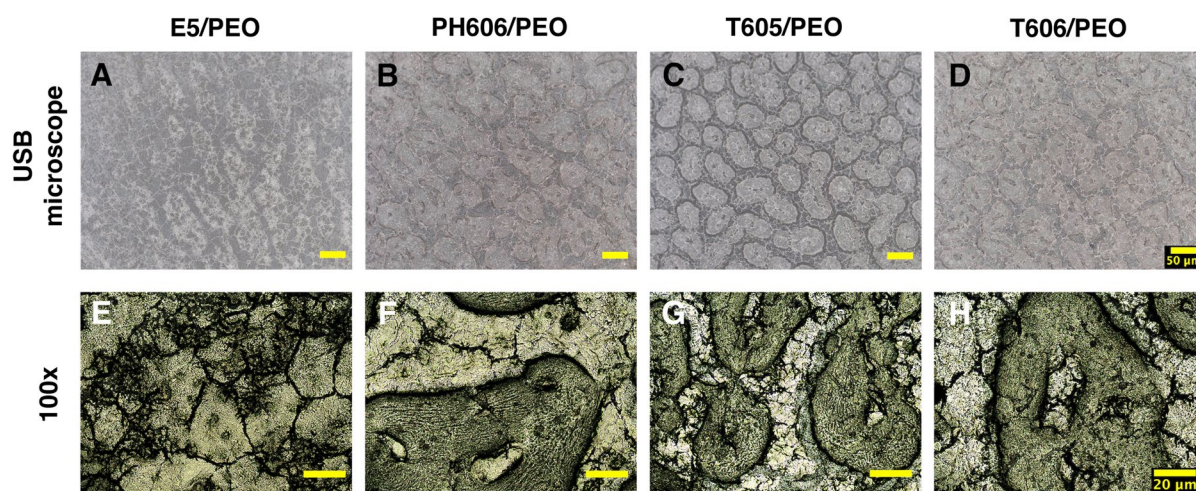Solutions with differing ratios of HPMC/PEO were subsequently prepared aimed at the investigation

Fig. 2 Macroscope (USB microscope) (**a–d**) and polarized light microscopy (**e–h**) images of the solvent-cast HPMC/PEO films following complete drying. The scale bar is 50 µm and 20 µm for the USB microscope and 100×magnifications, respectively
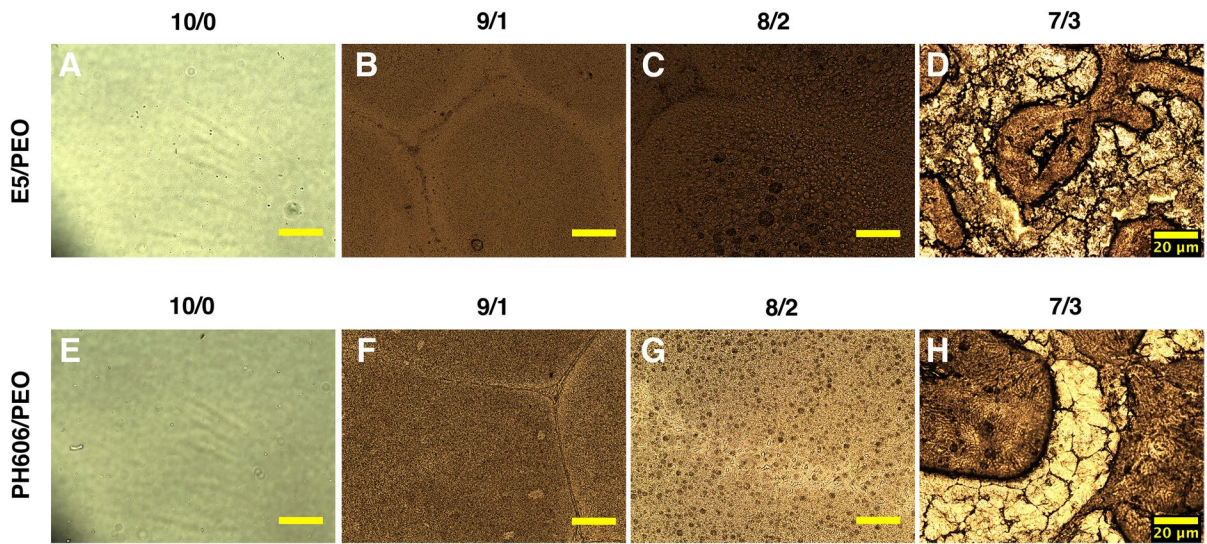
Fig. 3 Polarized light microscopy images of the E5/PEO (**a–d**) and PH606/PEO (**e–h**) solvent-cast films with differing ratios of PEO

of this aspect of microphase separation in more detail. The microscopic analysis revealed that the phase separation changed markedly for both the E5/PEO and PH606/PEO samples. Obvious microphase separation occurred at a ratio of 9/1, with HPMC particles that were comparable to the PEO nuclei. Moreover, the particles from the separated HPMC microphase dispersed in the PEO increased intensively with the increasing ratio of PEO. With respect to both the E5/PEO and PH606/PEO samples, the separated amorphous HPMC domains were significantly larger and were densely dispersed within the easily distinguishable crystal PEO phase. Moreover, a comparison of the 7/3 ratios for both the E5 and PH606 samples (Fig. 3d, h) revealed that the shape of the PEO crystals and their distribution throughout the film was not as regular for the E5/PEO as for the PH606/PEO sample. This observation may indicate the higher degree
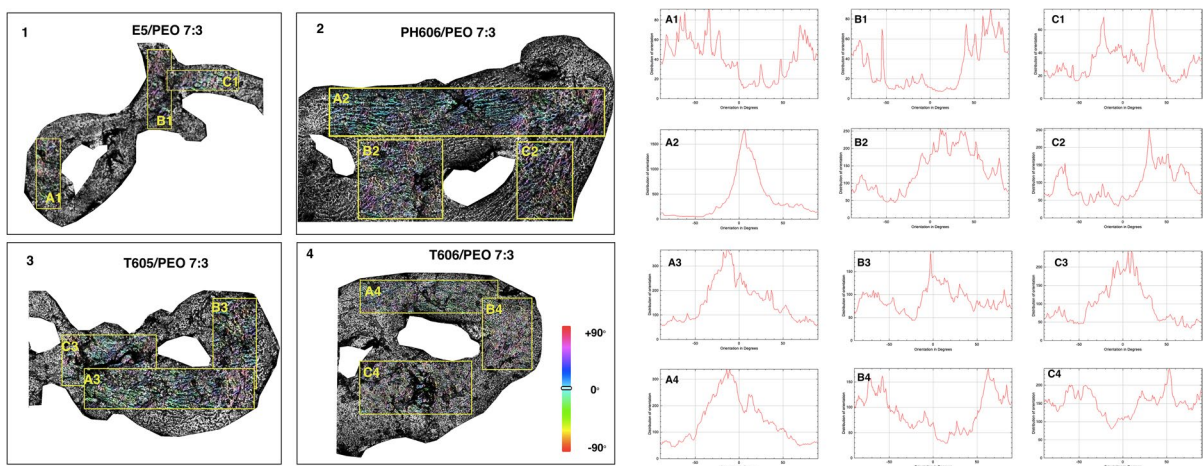
Fig. 4 Representative results of the analysis of the orientation and coherency of the PEO crystalline phase in the HPMC domains. Each frame (1–4) presents a typical HPMC domain cut from the polarized light microscopy image, three color-coded measured areas, and the corresponding histograms of the orientation distributions

of compatibility (miscibility) of the polymers in the E5/PEO formulation. The morphology of the PEO crystals was consistent with the results determined by Lovinger and Gryte (1976).

It is clear from the images shown in Fig. 3 that the PH606/PEO, T605/PEO, and T606/PEO sample HPMC domains exhibit a specific orientation in terms of the interconnections within the grains, whereas no evidence of anisotropy was observed from the E5/PEO images. This observation was partially confirmed via the plugin OrientationJ in ImageJ software (Fig. 4) which was used for the analysis of the local orientations of typical HPMC domain fragments. As can be seen from the histograms of the distribution of the local orientations and the color-coded maps, no defined peak was evident for the E5/PEO, whereas more or less narrow well-distinguishable peaks were observed for the PH606/PEO, T605/PEO, and T606/PEO samples. Despite the presence of isotropic or multimodal areas on the PH606/PEO, T605/PEO, and T606/PEO domains, the coherency was in most cases higher than that of the E5/PEO. This may indicate

differences in terms of the miscibility of the polymers due to variations in the interactions that occur between the PEO and the HPMC, as well as differing degrees of the interruption of the PEO crystalline phase by the HPMC.

DSC characterization

Figure 5 presents the DSC thermograms of various HPMC/PEO nanofibrous layer samples recorded at a heating/cooling rate of 15 °C/min. All the blended samples exhibited pronounced endothermic peaks during heating and sharp pronounced exothermic peaks during cooling. The exothermic peak corresponded to the cold crystallization temperature of the PEO, while the endothermic peak corresponded to the reported values of the PEO melting point (Nijenhuis et al. 1996; Money and Swenson 2013; Aydogdu et al. 2018; Meruva and Donovan 2020) The lowest exothermic peak and enthalpy of cold crystallization values were determined for the E5/PEO sample (35.82 °C and 27.33 J/g, respectively),

Fig. 5 DSC curves for the HPMCs/PEO (7/3) physical mixtures (**a**) and the nanofibrous layers (**b**) heated at 15 °C/min and subsequently cooled at 15 °C/min. The peaks that appear above the baseline represent the endothermic peaks
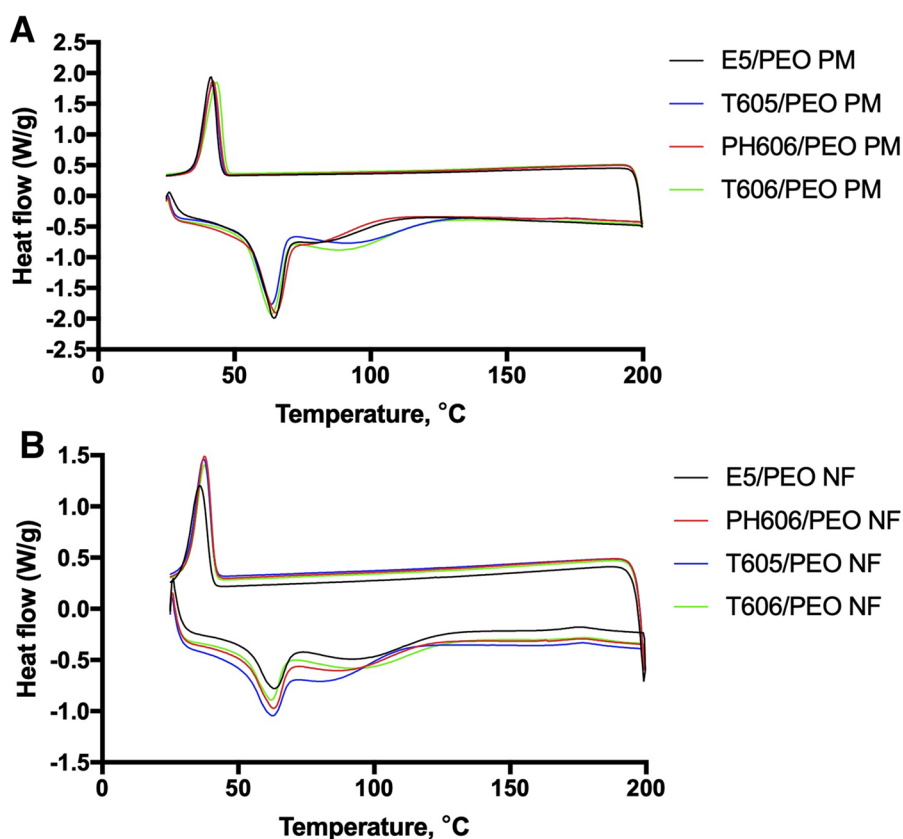
whereas the highest temperature and enthalpy of cold crystallization values were observed for the PH606/PEO sample. All the thermograms featured a broad peak at approx. 95 °C, which may indicate the dehydration of the humidity absorbed by the samples during storage. The comparative DSC analysis of the physical mixtures stored under normal conditions and the physical mixtures dried before measurement revealed the high degree of hygroscopicity of the materials, as evident from the DSC thermograms, i.e. the enthalpy of the melting of PEO changes significantly with increased water content. On the other hand, the glass transition temperature of the HPMC was not detected for any of the HPMCs during the measurement process, which is consistent with the observations reported earlier for the electrospun HPMC/PEO nanofibers (Balogh et al. 2016); the glass transition temperature of HPMC is reported as 155 °C in the literature (Nyamweya and Hoag 2000).

Due to the absence of detectable temperatures and enthalpies for the cold crystallization/melting of HPMC, a summary of these values with respect to the PEO of selected samples is presented in Table 2.

A noticeable trend is evident in the decrement of the temperature of the melting of PEO from the pure PEO powder toward the electrospun samples. Table 2 indicates an approximately 7% decrement for the physical mixtures and an approximately 10% decrement for the nanofibers. Moreover, the enthalpy of melting decreased dramatically in the same direction by up to 90% and the enthalpy of cold crystallization by up to 30%. The depression of the melting point may have been due to the inter-reference of the PEO crystallization process by the HPMC domains. Taken together, this appears to serve as a good indicator of the higher degree of interaction between PEO and HPMC in nanofibers (Rathna et al. 2011; Bianco et al. 2013). Similar observations have been reported previously for HPMC/PEO (Aydogdu et al. 2018) and PCL/PEO nanofibrous blends (Lowery et al. 2010). The lower temperature of the cold crystallization of PEO in the nanofibrous samples than in the physical mixtures comprises an important aspect. The depression of the cold crystallization temperature indicates the enhanced crystalline ability of PEO and appears to suggest that HPMC domains serve as nucleation sites for PEO (Li et al. 2012).

Mechanical properties of the nanofibrous layers

The properties of oral films are type-dependent (fast dissolving, gradual release, etc.). However, all the various types of films are required to fulfill certain property requirements, i.e. they should be thin, efficiently and rapidly dissolvable, have an acceptable taste, and, most importantly, must allow for the ease of handling during production and subsequent administration (Bala et al. 2013; Borges et al. 2015). Of the various properties, priority is accorded to the mechanical properties of the film, which should remain stable. Gupta and Kumar (Gupta and Kumar 2020), when describing the mechanical properties of oral films, suggested the ideal tensile and puncture properties of orodispersible films as follows: tensile strength of greater than 2 N/mm^2, elongation at break of greater than 10% and Young's modulus of less than 550 N/mm^2.

Figure 6A shows the typical tensile stress–strain curves of electrospun HPMC/PEO nanofibrous layers. Figure 6b compares Young's modulus of the various HPMC/PEO fibrous layers. The Young's modulus values of the E5/PEO and T605/PEO were comparable, i.e. 75.85 ± 13.91 and 75.42 ± 2.67 MPa, respectively. These values were significantly higher than that of the PH606/PEO and similar to that of the T606/PEO layers. Figure 6c compares the tensile stress of the materials at maximum load. The highest value, 2.12 ± 0.13 MPa, was determined for the T605/PEO layer; this was significantly higher than for the PH606/PEO and comparable to the E5/PEO and T606/PEO layers. Figure 6d shows the differences in the ultimate elongation of the tested materials before fracture. The lowest elongation value, i.e. $2.88 \pm 0.96\%$, was attained by the E5/PEO layer; this was lower than that of the T605/PEO ($5.48 \pm 0.86\%$) and significantly lower than those of the PH606/PEO ($6.43 \pm 0.94\%$) and T606/PEO ($7.05 \pm 0.68\%$) layers.

The relatively low Young's moduli of HPMC-containing formulations have been reported previously (Dott et al. 2013; Alopaeus et al. 2020; Shi et al. 2020). The comparison of the tensile properties of the materials tested in this study revealed a specific pattern of similarity between the materials spun from HPMCs with the same nominal viscosity. Generally, in terms of elastic deformation, the tensile behavior of E5/PEO and T605/PEO (5 mPa s) were similar, as was that of the PH606/PEO and T606/PEO (6 mPa s)

Table 2 DSC characterization of the pure polymers, nanofibrous samples, and physical mixtures of HPMC/PEO

Sample	Temperature of cold crystallization (°C)	Enthalpy of cold crystallization (J/g)	Melting temperature (°C)	Enthalpy of melting (J/g)
Nanofibrous samples				
E5/PEO NF	35.82	27.33	63.26	−17.69
PH606/PEO NF	37.66	30.20	62.95	−18.15
T605/PEO NF	37.40	29.75	62.42	−18.66
T606/PEO NF	37.65	28.51	61.97	−17.20
Physical mixtures				
E5/PEO	41.22	37.97	64.46	−46.96
PH606/PEO	42.00	37.79	65.18	−43.21
T605/PEO	41.75	37.43	63.45	−41.94
T606/PEO	43.53	36.94	67.37	−46.28
Pure polymer				
PEG 100 k powder	31.91	41.74	69.88	−174.11

The temperature and enthalpy of the cold crystallization/melting of PEO for selected samples

layers. However, a significant difference was evident concerning the E5/PEO layer in terms of the plastic deformation—the elongation at break of the E5/PEO was almost 2-times lower than that of the other tested layers. As suggested previously (Puppi et al. 2010), this may indicate the presence of a significant amount of the PEO crystalline phase, which hinders the mobility of the various polymer chains during stretching. Shi et al. (2020) reported the significant suppression of elongation with increases in the content of additives in the HPMC matrix, which was attributed to the possible agglomeration of the additives. As demonstrated by Shi et al. (2020), an increase in the HPMC chain length may act to enhance the mechanical properties due to the presence of a higher number of intermolecular bonds between the polymer chains. The results of the comparison of the elongations at a break in this study, however, suggest that higher viscosity (a higher molecular weight) plays a role primarily during the plastic deformation phase (see Fig. 6a, d).

Fourier-transform infrared spectroscopy (FTIR) and Raman Spectroscopy

The FTIR and Raman spectroscopy analyses served to provide important information on the macromolecular structures and functional groups of the HPMCs, which helped in terms of revealing the nature of the interactions between the various HPMCs and PEO.

Four HPMC powder samples were analyzed and compared using FTIR and two samples were analyzed by means of Raman spectroscopy.

Figure 7 shows the FTIR spectra obtained for the four differing HPMCs. The wave number of the OH (-hydroxy) strain was 3450 cm^{-1} and that of the C–H aliphatic strain was mainly 2906 cm^{-1}. The C–O–C stretching vibration of the PH606 was observed to comprise the strongest peaks (at 1052 and 947 cm^{-1}). The broad peak from 1200 cm^{-1} to 800 cm^{-1} was identified as a pyranose ring vibration. The smaller peaks at 1375 cm^{-1} and 1461 cm^{-1} corresponded to the symmetric and asymmetric bending vibrations of the –OCH$_3$ group (-methoxy), respectively. No noticeable differences were observed in the fingerprint region for the analyzed HPMC spectra (Fig. 7c). The FTIR spectra obtained for the HPMCs under study were consistent with the spectra presented in the literature (Akinosho et al. 2013; Aydogdu et al. 2018).

Raman spectroscopy, which is generally more sensitive to C–H stretching, was used to define the potential differences that were not determined via the FTIR analysis. The spectra of two HPMCs with enlarged CH stretching regions are shown in Fig. 8.

The comparison of the Raman spectra in Fig. 8 revealed a slight difference in the signal intensity primarily in the CH stretching region. The most intensive peaks at 2840, 2936, and 2895 were assigned to symmetric and asymmetric CH$_2$ stretching and the acyclic CH groups, respectively. The shoulder at

around 2980 was assigned to asymmetric CH$_3$ stretching (Socrates 2001). The Raman spectra revealed differences in the structures of the analyzed samples, mainly in terms of the linearity and length of the aliphatic chains. The signal intensity differences suggest that the E5 macromolecules evince a more branched structure and are generally shorter. On the other hand, PH606 is assumed to have longer and more linear macromolecules. These proposed properties are consistent with the fact that E5 has a lower viscosity, i.e., molecular weight, than PH606.

Conclusion

The use of nanofibers as ODFs has several advantages including relatively simple and inexpensive

production, very fast solubility, the absence of residual solvents, simple modifiability, etc. On the other hand, their large-scale use is limited primarily due to their poor mechanical properties and long-term stability issues.

This paper aimed to show that even a relatively small variation in the parameters of the input polymers can significantly affect the mechanical properties of nanofibrous layers. We selected a polymer that is used widely in the pharmaceutical industry, HPMC, for the preparation of the ODF films. Two groups of polymers with the same inherent viscosity produced by different manufacturers were tested with respect to a range of parameters. The study revealed that while the higher viscosity group evinced very similar characteristics for both polymers, this was not the case for the lower viscosity
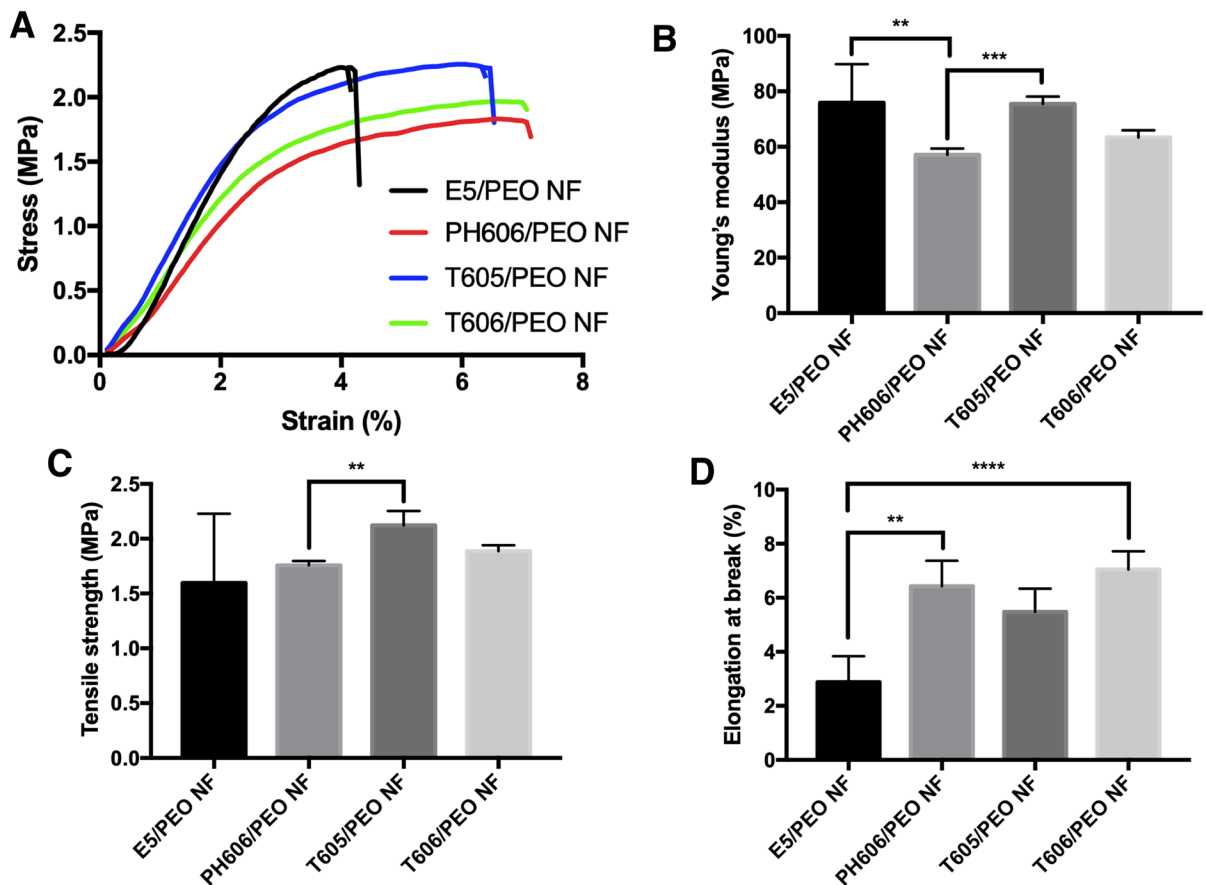
Fig. 6 Tensile properties of the electrospun HPMC/PEO layers. Representative stress–strain curves (**a**), Young's modulus (**b**), tensile stress at maximum load (**c**) and elongation at break (**d**) of the various electrospun HPMC/PEO layers. The asterisks (*) indicate a statistically significant difference ($p < 0.05$) between the two materials; none of the other comparisons were statistically significant
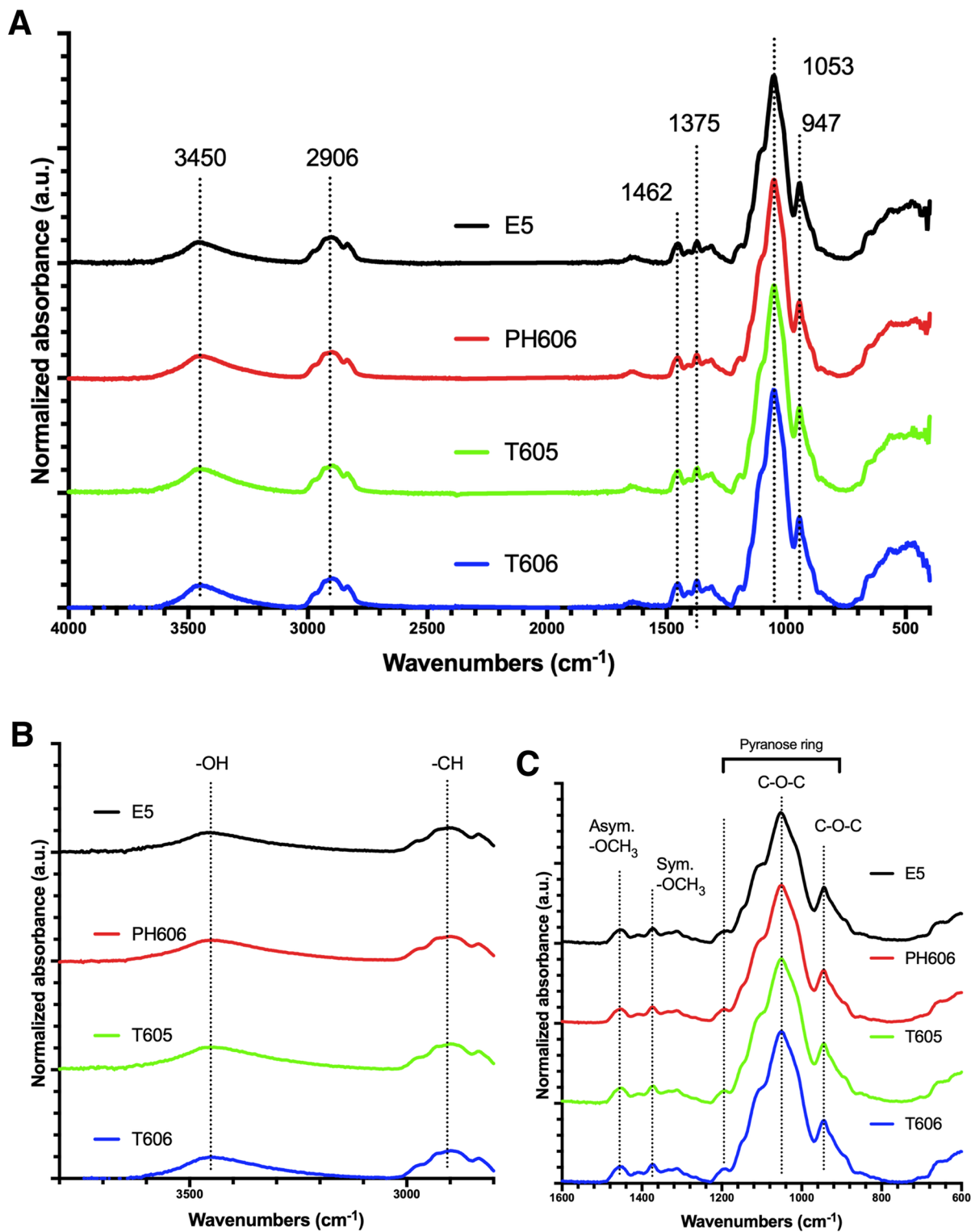
Fig. 7 FTIR spectra of the pure HPMC powders (panel **A**). Magnified FTIR spectra of HPMC with a wave number range of 2800–3800 cm^{-1} (panel **B**) and with a wave number range of 600–1600 cm^{-1} (panel **C**)

Fig. 8 Superimposed Raman spectra of pure HPMC Methocel E5 and Pharmacoat 606 powder samples with a chemical structure of HPMC in the upper right corner of the figure. The spectra have been enlarged in the CH–OH region to highlight the differences
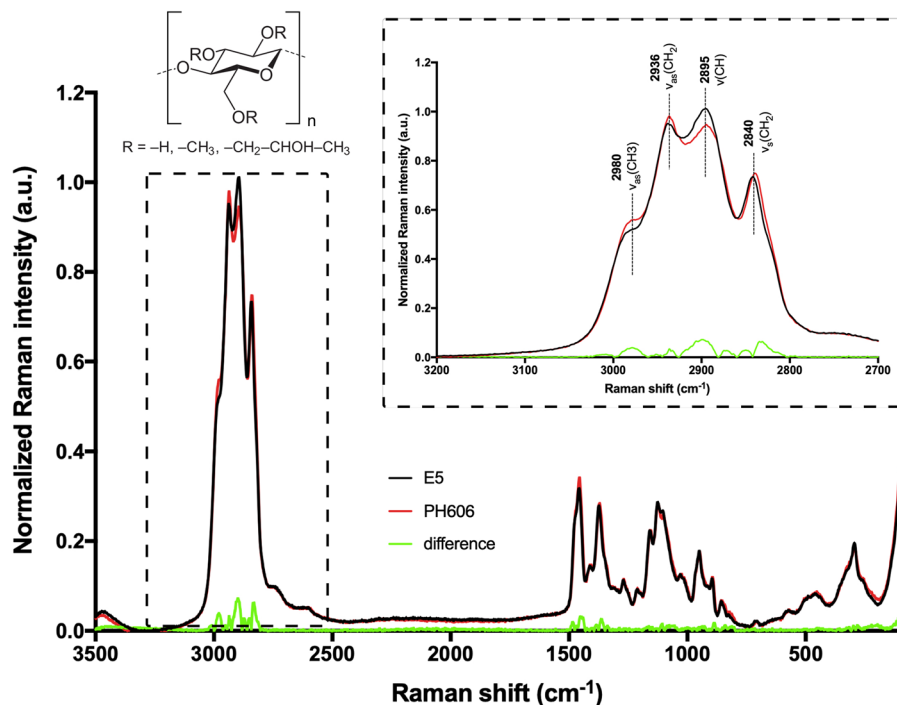
group. Even though no significant difference was observed between the two polymers, the mechanical properties of Methocel E5 were approximately half as good *as* the rest of the tested polymers. The calorimetric measurements did not reveal any areas of significant crystallinity, nor did the morphology and infrared spectroscopy suggest any significant differences. The examination of the optical microscope images of the layers produced by the solvent casting method confirmed the orderliness of certain regions in the Methocel E5 combined with PEO compared to the other HPMCs.

The Raman spectroscopy analysis suggested that the main differences between the samples consisted of the linearity and length of the aliphatic chains of the macromolecules. The E5 macromolecules were assumed to have more branched and generally shorter aliphatic chains, while the PH606 was assumed to have longer and more linear macromolecules. Thus, it is reasonable to speculate that these slight differences can affect interactions between the macromolecules and thus lead to a significant deterioration in the mechanical properties of the fabricated layer.

The characterization of the input polymers is of significant importance. Even a slight change in the

isomerism can significantly affect the parameters of the fabricated layer. This study demonstrated a series of analytical methods that enhance the understanding of the behavior of mixed polymer solutions intended for electrostatic spinning.

Declarations

Conflict of interest The authors have no relevant financial or non-financial interests to disclose.

Ethics approval Not applicable.

Consent to participate Not applicable.

Consent for publication All authors whose names appear on the submission made substantial contributions to the conception or design of the work; or the acquisition, analysis, or interpretation of data; drafted the work or revised it critically for important intellectual content; approved the version to be published; and agree to be accountable for all aspects of the work in ensuring that questions related to the accuracy or integrity of any part of the work are appropriately investigated and resolved.

References

Akinosho H, Hawkins S, Wicker L (2013) Hydroxypropyl methylcellulose substituent analysis and rheological properties. Carbohydr Polym 98:276–281. https://doi.org/10.1016/j.carbpol.2013.05.081

Alopaeus JF, Hellfritzsch M, Gutowski T et al (2020) Mucoadhesive buccal films based on a graft co-polymer – a mucin-retentive hydrogel scaffold. Eur J Pharm Sci 142:105142. https://doi.org/10.1016/j.ejps.2019.105142

Aydogdu A, Sumnu G, Sahin S (2018) A novel electrospun hydroxypropyl methylcellulose/polyethylene oxide blend nanofibers: morphology and physicochemical properties. Carbohydr Polym 181:234–246. https://doi.org/10.1016/j.carbpol.2017.10.071

Bahrainian S, Abbaspour M, Kouchak M, Taghavi Moghadam P (2017) A review on fast dissolving systems: from tablets to nanofibers. Jundishapur J Nat Pharm Prod 12:e34267. https://doi.org/10.5812/jjnpp.34267

Bala R, Khanna S, Pawar P, Arora S (2013) Orally dissolving strips: a new approach to oral drug delivery system. Int J Pharm Investig 3:67–76. https://doi.org/10.4103/2230-973x.114897

Balogh A, Farkas B, Verreck G et al (2016) AC and DC electrospinning of hydroxypropylmethylcellulose with polyethylene oxides as secondary polymer for improved drug dissolution. Int J Pharm 505:159–166. https://doi.org/10.1016/j.ijpharm.2016.03.024

Bianco A, Calderone M, Cacciotti I (2013) Electrospun PHBV/PEO co-solution blends: microstructure, thermal and mechanical properties. Mater Sci Eng C 33:1067–1077. https://doi.org/10.1016/j.msec.2012.11.030

Bin LK, Tan YTF, Peh KK (2014) Effect of polymer, plasticizer and filler on orally disintegrating film. Drug Dev Ind Pharm 40:110–119. https://doi.org/10.3109/03639045.2012.749889

Birer M, Acartürk F (2021) Electrospun orally disintegrating film formulation of telmisartan. Pharm Dev Technol 26:661–672. https://doi.org/10.1080/10837450.2021.1916031

Borges AF, Silva C, Coelho JFJ, Simões S (2015) Oral films: current status and future perspectives: I-Galenical development and quality attributes. J Control Release 206:108–121. https://doi.org/10.1016/j.jconrel.2015.03.012

Bukhary H, Williams GR, Orlu M (2018) Electrospun fixed dose formulations of amlodipine besylate and valsartan. Int J Pharm 549:446–455. https://doi.org/10.1016/j.ijpharm.2018.08.008

Council of Europe (2019) European pharmacopoeia, 10th edn. Council of Europe, Strasbourg

Dott C, Tyagi C, Tomar LK et al (2013) A mucoadhesive electrospun nanofibrous matrix for rapid oramucosal drug delivery. J Nanomater 2013:3–22. https://doi.org/10.1155/2013/924947

Effiong Daniel Ekpa, Umoh Romanus Asuquo, Akpabio Akwaowo Elijah et al (2020) The oral film delivery-application of nanotechnology and potential in medication adherence. GSC Biol Pharm Sci 11:034–051. https://doi.org/10.30574/gscbps.2020.11.3.0154

Gupta MS, Kumar TP (2020) Characterization of orodispersible films: an overview of methods and introduction to a new disintegration test apparatus using LDR–LED sensors. J Pharm Sci 109:2925–2942. https://doi.org/10.1016/j.xphs.2020.06.012

Hoffmann EM, Breitenbach A, Breitkreutz J (2011) Advances in orodispersible films for drug delivery. Expert Opin Drug Deliv 8:299–316. https://doi.org/10.1517/17425247.2011.553217

Irfan M, Rabel S, Bukhtar Q et al (2016) Orally disintegrating films: a modern expansion in drug delivery system. Saudi Pharm J 24:537–546. https://doi.org/10.1016/j.jsps.2015.02.024

Li Y, Chen C, Li J, Sun XS (2012) Isothermal crystallization and melting behaviors of bionanocomposites from poly(lactic acid) and TiO2 nanowires. J Appl Polym Sci 124:2968–2977. https://doi.org/10.1002/app.35326

Lin T, Wang X (2013) Needleless electrospinning of nanofibers: technology and applications. CRC Press, Boca Raton

Lovinger AJ, Gryte CC (1976) The morphology of directionally solidified Poly(ethylene oxide) Spherulites. Macromolecules 9:247–253. https://doi.org/10.1021/ma60050a014

Lowery JL, Datta N, Rutledge GC (2010) Effect of fiber diameter, pore size and seeding method on growth of human dermal fibroblasts in electrospun poly(ε-caprolactone) fibrous mats. Biomaterials 31:491–504. https://doi.org/10.1016/j.biomaterials.2009.09.072

Mahboob MBH, Riaz T, Jamshaid M et al (2016) Oral films: a comprehensive review. Int Curr Pharm J 5:111–117. https://doi.org/10.3329/icpj.v5i12.30413

Meruva S, Donovan MD (2020) Polyethylene Oxide (PEO) molecular weight effects on abuse-deterrent properties of matrix tablets. AAPS PharmSciTech 21:28. https://doi.org/10.1208/s12249-019-1565-y

Money BK, Swenson J (2013) Dynamics of poly(ethylene oxide) around its melting temperature. Macromolecules 46:6949–6954. https://doi.org/10.1021/ma4003598

Nijenhuis AJ, Colstee E, Grijpma DW, Pennings AJ (1996) High molecular weight poly(L-lactide) and poly(ethylene oxide) blends: thermal characterization and physical properties. Polymer (Guildf) 37:5849–5857. https://doi.org/10.1016/S0032-3861(96)00455-7

Nyamweya N, Hoag SW (2000) Assessment of polymer-polymer interactions in blends of HPMC and film forming polymers by modulated temperature differential scanning calorimetry. Pharm Res 17:625–631. https://doi.org/10.1023/A:1007585403781

Orlu M, Ranmal SR, Sheng Y et al (2017) Acceptability of orodispersible films for delivery of medicines to infants and preschool children. Drug Deliv 24:1243–1248. https://doi.org/10.1080/10717544.2017.1370512

Paaver U, Heinämäki J, Laidmäe I et al (2015) Electrospun nanofibers as a potential controlled-release solid dispersion system for poorly water-soluble drugs. Int J Pharm 479:252–260. https://doi.org/10.1016/j.ijpharm.2014.12.024

Preis M (2015) Orally disintegrating films and mini-tablets—innovative dosage forms of choice for pediatric use. AAPS PharmSciTech 16:234–241. https://doi.org/10.1208/s12249-015-0313-1

Puppi D, Piras AM, Detta N et al (2010) Poly(lactic-co-glycolic acid) electrospun fibrous meshes for the controlled release of retinoic acid. Acta Biomater 6:1258–1268. https://doi.org/10.1016/j.actbio.2009.08.015

Rathna GVN, Jog JP, Gaikwad AB (2011) Development of non-woven nanofibers of egg albumen-poly (vinyl alcohol) blends: influence of solution properties on morphology of nanofibers. Polym J 43:654–661. https://doi.org/10.1038/pj.2011.34

Samprasit W, Akkaramongkolporn P, Ngawhirunpat T et al (2015) Fast releasing oral electrospun PVP/CD nanofiber mats of taste-masked meloxicam. Int J Pharm 487:213–222. https://doi.org/10.1016/j.ijpharm.2015.04.044

Shi SC, Chen TH, Mandal PK (2020) Enhancing the mechanical and tribological properties of cellulose nanocomposites with aluminum nanoadditives. Polymers (Basel) 12:1246. https://doi.org/10.3390/POLYM12061246

Slavkova M, Breitkreutz J (2015) Orodispersible drug formulations for children and elderly. Eur J Pharm Sci 75:2–9. https://doi.org/10.1016/j.ejps.2015.02.015

Socrates G (2001) Infrared and Raman characteristic group frequencies. Tables and charts. Wiley, Chichester

Švára D, Kopřivová B, Picek T et al (2022) The impact of the lamination pressure on the properties of electrospinned nanofibrous films. Eur J Pharm Sci 173:106170. https://doi.org/10.1016/j.ejps.2022.106170

Tort S, Acartürk F (2016) Preparation and characterization of electrospun nanofibers containing glutamine. Carbohydr Polym 152:802–814. https://doi.org/10.1016/j.carbpol.2016.07.028

Visser JC, Eugresya G, Hinrichs WLJ et al (2017) Development of orodispersible films with selected Indonesian medicinal plant extracts. J Herb Med 7:37–46. https://doi.org/10.1016/j.hermed.2016.10.002